

Structural coherence and ferroelectricity decay in submicron- and nano-sized perovskites

V. Petkov,^{1,*} V. Buscaglia,^{2,†} M. T. Buscaglia,² Z. Zhao,³ and Y. Ren⁴

¹*Department of Physics, Central Michigan University, Mount Pleasant, Michigan 48859, USA*

²*Institute for Energetics and Interphases, CNR, Via De Marini 6, I-16149 Genoa, Italy*

³*Institute of Inorganic Chemistry, University of Stockholm, S10691 Stockholm, Sweden*

⁴*Advanced Photon Source, Argonne National Laboratory, Argonne, Illinois 60439, USA*

(Received 2 March 2008; revised manuscript received 5 June 2008; published 11 August 2008)

Understanding the loss of ferroelectricity in submicron- and nano-sized perovskites is an issue that has been debated for decades. Here we report results from a high-energy x-ray diffraction (XRD) study on a prime example of the perovskite's family, BaTiO₃ ceramics with a grain size ranging from 1200 to 5 nm. We find that the loss of ferroelectricity in submicron- and nano-sized BaTiO₃ has an intrinsic origin related to the increased atomic positional disorder in spatially confined physical systems. Our results imply that no particular critical size at which ferroelectricity in BaTiO₃, in particular, and perovskites, in general, is completely lost exists. Rather it weakens exponentially with the decreasing of their physical size. Smart technological solutions are needed to bring it back.

DOI: [10.1103/PhysRevB.78.054107](https://doi.org/10.1103/PhysRevB.78.054107)

PACS number(s): 61.43.-j, 81.07.Bc

I. INTRODUCTION

Ferroelectric materials of the perovskite family ABO_3 , where $A = \text{Ba, Sr, and Pb}$, and $B = \text{Ti and Zr}$, are extensively used in electronic industry for fabrication of multilayer capacitors, piezoelectric transducers, pyroelectric elements, and ferroelectric memories.^{1,2} With these technologies moving quickly toward smaller scales, electronic devices are already shrunk to nanometer sizes. Unfortunately, such a reduction in the physical size of perovskite ferroelectrics results in a dramatic deterioration of one of their most useful properties, in particular a dramatic reduction in the spontaneous polarization.³ In bulk ceramics a progressive suppression of the spontaneous polarization and a reduction in the dielectric constant are observed when the grain size is reduced already below 1 μm .^{4,5} The suppression seems to be full when the grain size gets down to 30 nm since ferroelectric hysteresis loops no longer show evidence of domain switching even when electric fields of 60 kV/cm are applied.⁶ High-quality epitaxial ABO_3 films have been reported to exhibit a similar behavior retaining ferroelectricity down to a thickness of a few nanometers only.^{7,8} Several studies aimed at understanding the observed ferroelectricity “size” effect have been conducted. Classical, phenomenological thermodynamic theory studies (Landau-Ginzburg-Devonshire approach) concluded that the effect may be viewed as a phase transition from a ferroelectric to a paraelectric state taking place at a critical system size of a few to a few tens of nanometers.⁹ Another point of view asserts the presence of a thin layer, referred to as “dead,” lacking in or with a greatly reduced spontaneous polarization and low dielectric constant at the grain boundaries of bulk ceramics and the electrode/ferroelectric interface in supported thin films/capacitors.^{4,10,11} The layer has been explained in terms of a depolarization field arising from the inhomogeneity of charge distribution at the surface/interface discontinuity.¹² The likely presence of structural imperfections such as oxygen vacancies, dislocations, disorder, etc. at the film interfaces and/or grain boundaries has been widely discussed as well.¹¹⁻¹³ However, the loss of fer-

roelectricity in both thin perovskite films and bulk ceramics has also been found to be accompanied by a profound hardening of the so-called soft phonon mode.¹²⁻¹⁴ Phonon modes are the elementary vibrations of crystalline lattices, implying that not just the increased surface in submicron- and nano-sized perovskites but the way atoms interact inside them may be at the root of the unwanted ferroelectricity loss. Here we explore this aspect of the size effect using high-energy x-ray diffraction (XRD) and atomic pair distribution function (PDF) analysis. The approach has already proven to be very successful in studying the atomic arrangement inside materials of very limited structural coherence, including nanosized crystals.¹⁵ We concentrated on a prime example of the perovskite ferroelectrics family, BaTiO₃. We found that the deterioration of spontaneous polarization in submicron- and nano-sized BaTiO₃ is indeed a typical decay of a bulk material's property due to a gradual weakening of the longer-range interatomic correlations that are necessary for that property to exist. The weakening may be understood easily if considered in terms of the famous “uncertainty principle”; in this case it is a gradual increase in the root-mean-square (rms) fluctuations of atomic positions taking place when the size of physical systems is reduced gradually down to the nanometer scale. In other words, we found that the deterioration of spontaneous polarization in submicron- and nano-sized perovskites has an intrinsic origin related to the spatial confinement of the system.

II. EXPERIMENT RATIONALE AND RESULTS

At high temperature, BaTiO₃ has a centrosymmetric cubic structure and is paraelectric. Between room temperature and 393 K, known as the ferroelectric Curie temperature, the material possesses a tetragonal-type structure, below 278 K the structure is orthorhombic, and below 183 K—rhombohedral.¹⁶ Fragments of the cubic and the technologically important tetragonal phases of BaTiO₃ are presented in Fig. 1. The structural pattern is characteristic for all ABO_3 perovskites. It features a three-dimensional (3D) network of

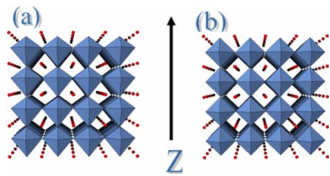


FIG. 1. (Color online) Fragments of the tetragonal (a) and cubic (b) modifications of BaTiO_3 . Both modifications are three-dimensional networks of corner-sharing Ti-O_6 octahedra (blue diamonds). The network cavities are occupied by Ba atoms (red dots). With tetragonal BaTiO_3 the oxygen octahedra are slightly elongated and Ti atoms displaced off their centers, giving rise to a polar axis of symmetry (Z). The octahedra are fairly regular in cubic BaTiO_3 .

$B\text{-O}_6$ ($B=\text{Ti}$) octahedra with A (Ba) atoms occupying the network channels. In the cubic phase the oxygen octahedra are fairly regular, and the centers of positive (metal) and negative (oxygen) charges coincide. As a result no electrical dipole is present. In the tetragonal phase Ti cations are displaced with respect to the center of the oxygen octahedra and the latter are slightly distorted. As a result, the centers of the positive and negative charges are offset. The magnitude of these static displacements from the vertices of the nonpolar (cubic) lattice is fairly small, only about $0.02(5)$ Å,¹⁶ but large enough to generate a substantial electric-dipole moment. In bulk tetragonal perovskites, the distorted Ti-O_6 octahedra are coupled into a three-dimensional periodic lattice. Accordingly, their dipole moments exhibit a long-range order, giving rise to a large spontaneous polarization. The direction of polarization may be switched between equivalent states by the application of an external electric field, rendering the material a typical ferroelectric. Due to their large response to an external electric field, ferroelectric materials have a large (i.e., hundreds to a few thousands) dielectric constant.

Recently we studied 5 nm BaTiO_3 particles that have “lost” their ferroelectricity, as manifested by the rather low (~ 100) dielectric constant. We found that the Ti-O_6 octahedra in this nanosized perovskite are indeed distorted (i.e., polar) but the tetragonal lattice distortions remain local and correlated over distances of about 1.5 nm only. As a result, on average, the material exhibits a nonpolar, i.e., a cubic-type like structure and a low dielectric constant.¹⁷ Here we follow up on this study, looking up for the presence of a similar pattern in a series of BaTiO_3 ceramics with a grain size ranging from 1200 to 30 nm and dielectric constants varying from ~ 2520 to ~ 350 , respectively. The samples were obtained by spark plasma sintering, as described in Ref. 11. The 3D structure of the ceramics was determined by high-energy XRD and atomic PDF analysis. The experiments were carried out at the beamline 11-ID-C (Advanced Photon Source, Argonne National Laboratory) using x rays of energy 115.232 keV ($\lambda=0.1076$ Å) at room temperature. X rays of higher energy were used to obtain diffraction data to higher values of the wave vector Q , which is important for the success of PDF analysis. Experimental diffraction patterns are shown in Fig. 2. Bragg peaks in the XRD pattern for the 1200 nm sample may be unambiguously indexed in terms of the tetragonal perovskite lattice shown in Fig. 1. Bragg peaks

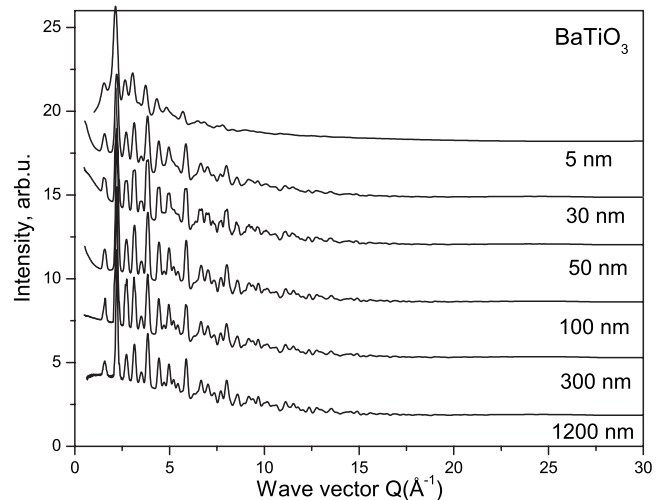


FIG. 2. Experimental XRD patterns of submicron- and nano-sized BaTiO_3 .

in XRD patterns of the other samples smear out with the diminishing of particle size, making it increasingly difficult to differentiate between the tetragonal and cubic modifications of BaTiO_3 .^{11,17} However, when considered in terms of the corresponding atomic PDFs, the same XRD data lend themselves to an accurate structure characterization.¹⁸ The experimental atomic PDFs $G(r)$ are shown in Fig. 3. That for not-sintered 5 nm BaTiO_3 particles, resulted from a previous study of ours,¹⁷ is shown as well. The PDF $G(r)=4\pi r[\rho(r)-\rho_0]$, where $\rho(r)$ and ρ_0 are the local and average atomic number densities, respectively, and r is the radial distance. It peaks at distances separating frequently occurring pairs of atoms and thus reflects the 3D atomic arrangement of materials. Here it should be noted that for a material comprising of n atomic species, a single diffraction experiment yields a $G(r)$, which is a weighted sum of $n(n+1)/2$ partial PDFs

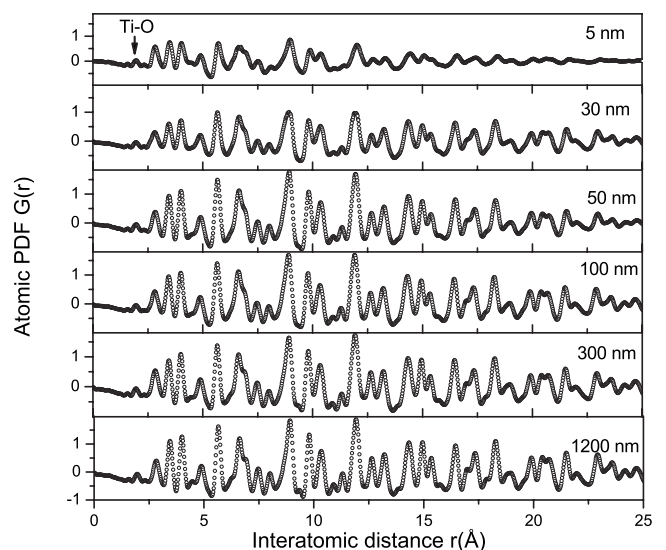


FIG. 3. Experimental atomic PDFs for submicron- and nano-sized BaTiO_3 shown on the same scale so that the physical system size related changes in them are monitored easier. The PDF peak reflecting first neighbor Ti-O correlations is marked with an arrow.

whose weights depend on the relative concentration and x-ray scattering power of the atomic species involved.¹⁸ The contribution of Ba-Ba, Ba-Ti, and Ti-Ti atomic pairs to the PDFs shown in Fig. 3 are 30%, 24%, and 5%, respectively, rendering the experimental data particularly sensitive to the metal-metal atomic correlations in perovskites.

III. DISCUSSION

As can be seen in Fig. 3, all experimental PDFs have a first peak positioned at approximately 1.98(2) Å, which is close to the average Ti-O first neighbor distance observed in bulk BaTiO₃, indicating that the nanosized samples we study are, like bulk BaTiO₃, built of Ti-O₆ octahedral units. As may be expected the PDF for the 1200 nm sample, which shows a large dielectric constant, could not be described well in terms of a model based on the paraelectric cubic [space group (SG) *Pm-3m*] phase of BaTiO₃. The model parameters were refined to a lattice parameter $a=3.999(1)$ Å with Ba at (0,0,0), Ti at (0.5,0.5,0.5), and oxygen at (0,0.5,0.5) positions in the cubic lattice, yielding an agreement factor $R_{wp}=20\%$. The fit was done over a range of r values from 1 to 30 Å. The experimental PDF was much better described ($R_{wp}=14\%$) by a model based on a tetragonal (noncentrosymmetric) lattice (SG *P4mm*) with parameters $a=3.987(1)$ Å and $c=4.017(1)$ Å, with Ba atoms at (0,0,0), Ti at (0.5,0.5,0.472), and oxygen atoms at O1(0.5,0.5,-0.105) and O2(0,0.5,0.480) positions inside the unit cell. For comparison the structure of bulk tetragonal BaTiO₃ has been described in terms of a lattice with parameters $a=3.9909(1)$ Å and $c=4.0352(1)$ Å, Ba at (0,0,0), Ti at (0.5,0.5,0.522), O1(0.5,0.5,-0.022), and O2(0,0.5,0.49).¹⁶ Also, our previous studies showed¹⁷ that those parameters for the 5 nm sample are $a=3.997(6)$ Å and $c=4.0851(7)$ Å, Ba at (0,0,0), Ti at (0.5,0.5,0.47), O1(0.5,0.5,-0.13), and O2(0,0.5,0.49). Our present and previous results clearly show that the displacement of both Ti and O1 (apical) oxygen atoms off the vertices of the ideal perovskite lattice increases with diminishing physical system/sample size. This result is well in line with the findings of independent extended x-ray-absorption fine structure (EXAFS) and traditional XRD/Rietveld studies on BaTiO₃ samples of substantially reduced length of structural coherence.¹⁹ The increased distortion in Ti-O₆ units (i.e., the increased displacement in the centers of the positive and negative charges) should result in an enhancement of their dipole moment. As our data for the dielectric constants show, however, the likely enhancement of local dipole moments in nano-sized BaTiO₃ does not translate into an enhancement of the net spontaneous polarization. The reasons for this counterintuitive behavior are discussed below.

As can also be seen in Fig. 3, the peaks in the experimental PDFs become increasingly broader with the decrease in particle size, signaling an increasing structural disorder. The disorder is very strong, reducing the length of structural coherence in the perovskites studied, that is measured by the real-space distance from which the experimental PDFs decay to zero, to distances substantially shorter than the average grain/particle size (e.g., the structural coherence length is

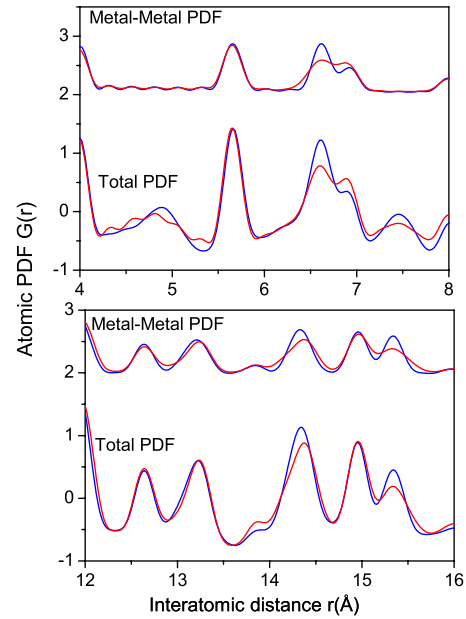


FIG. 4. (Color online) Model total and metal-metal partial atomic PDFs for BaTiO₃ shown over two regions of interatomic distances. The data are computed on the basis of a cubic-type (line in blue/dark gray) and tetragonal-type (line in red/light gray) structures.

only about 2 nm in the 5 nm sample; see Fig. 3). Such disorder may not be described well within the crystallographic constraints of either the cubic or tetragonal structure models alone, as discussed in our previous study.¹⁷ This prompted us to concentrate on some of the model's most distinct structural features instead. As such we considered the distribution of metal atoms (i.e., the distribution of positive charge) on the vertices of the crystalline lattice since it reflects well the ferroelectric behavior of perovskites. Note that such a consideration is difficult to be done in reciprocal space since, in contrast to PDF peaks, Bragg peaks are due to atomic planes and not to particular types of atomic pairs.

The spatial distribution of Ti (*B*-type) atoms is pretty uniform in the cubic phase and not so in the tetragonal one where they are shifted off the centers of oxygen octahedra, rendering them polar. On the other hand, the distribution of Ba (*A*-type) metal atoms barely changes between the two crystalline modifications of perovskites. Model total and metal-metal partial PDFs computed on the basis of the cubic and tetragonal structures of BaTiO₃ are shown in Fig. 4. The computations were done using the set of refined structural parameters reported above. As can be seen in the figure, the PDF peaks pertaining to metal-metal atomic pairs are definitely sharper for the cubic than for the tetragonal-based model reflecting the more uniform distribution of Ti atoms in the former. As a result, the higher- r shoulder of the PDF doublet at 6.5 Å is more pronounced with the tetragonal structure model than with the cubic one. Also, the ratio of the PDF peaks at 14.3 Å and 14.9 Å is quite different for the two models. It is about 1.2 to 1 for the almost uniform (non-polar) and about 1 to 1 for the quite nonuniform (polar) distribution of Ti atoms on the vertices of the perovskite lattice. Note the PDF peaks (e.g., those at 5.6 and 13.2 Å),

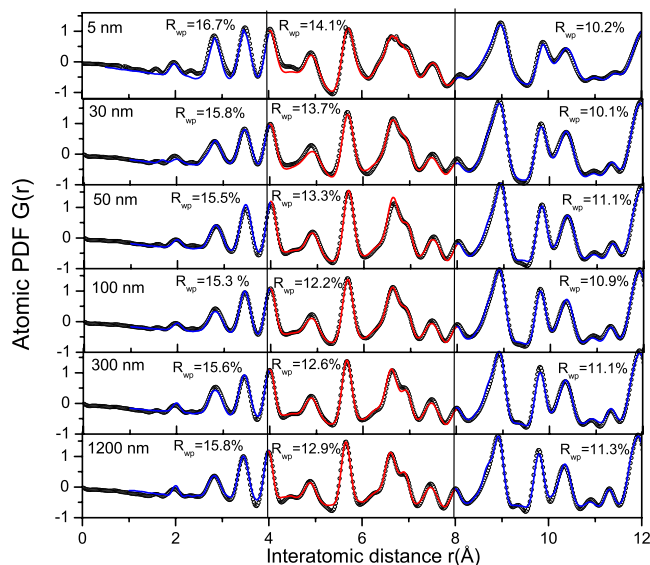


FIG. 5. (Color online) Low- r part of the experimental (symbols) and model (solid line) PDFs for submicron- and nano-sized BaTiO₃. The individual PDFs shown here are blown out so that the details in them are seen easier. The model data are computed on the basis of a tetragonal-type structure. The agreement factors, R_{wp} , computed over ranges of r values from 0–4 Å (line in blue), 4–8 Å (line in red), and 8–12 Å (line in blue) are reported as well. Note the agreement factors for the 0–4 Å range of data are somewhat worsened due to the fact that the PDF experimental artifacts tend to pile up at low- r values. The vertical lines are a guide to the eye.

which do not pertain to Ti-related interatomic pairs, do not show substantial differences between the tetragonal and cubic-type structure models, as it should. As the data presented in Figs. 5 and 6 show, the tetragonal-type atomic arrangement is consistently better than the cubic one in describing all important details in the low- r region (0–12 Å) of the experimental PDF data, in particular the characteristic shape of the PDF doublet at 6.5 Å. The result clearly shows that at room temperature the nonuniform, i.e., polar-type, distribution of Ti atoms is present in all submicron- and nano-sized BaTiO₃ samples studied. The result is fully in line with the findings of local probe/spectroscopy techniques such as Raman,²⁰ which have repeatedly shown that local tetragonal-type distortions are always present in small sized perovskites. By contrast, the intensity ratio of the PDF peaks positioned at 14.3 and 14.9 Å changes from 1 to 1 for the 1200 nm sample to 1.19 to 1 for the 5 nm sample, as the data presented in Fig. 7 show. This result may be understood in the following way: the distorted/polar Ti-O₆ octahedra are coupled over long-range distances in a 3D lattice in the 1200 nm sample, as in bulk BaTiO₃. As a result both materials are ferroelectric and exhibit a large net polarization (i.e., large dielectric constants). When the physical size of BaTiO₃ is reduced below approximately 1 μm, the Ti-O₆ octahedra remain and are likely to get even somewhat more distorted but progressively lose its long-range order. The octahedra obviously still form a perovskite-type lattice (see the fits in Figs. 4 and 5) but the periodicity of this lattice becomes less and less extended. As a result the material gradually loses its

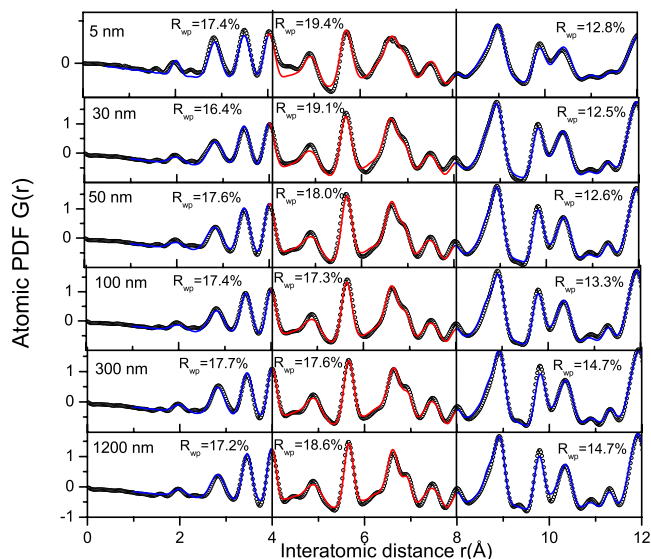


FIG. 6. (Color online) Low- r part of the experimental (symbols) and model (solid line) PDFs for submicron- and nano-sized BaTiO₃. The individual PDFs shown here are blown out so that the details in them are seen easier. The model data are computed on the basis of a cubic-type structure. The agreement factors, R_{wp} , computed over ranges of r values from 0–4 Å (line in blue), 4–8 Å (line in red), and 8–12 Å (line in blue) are reported as well. The vertical lines are a guide to the eye.

ability to show a large net polarization, i.e., loses its ferroelectricity. The way this process proceeds is summarized in Fig. 8. As can be seen in the figure, both the weakening of the long-range periodicity of the spatial arrangement of the

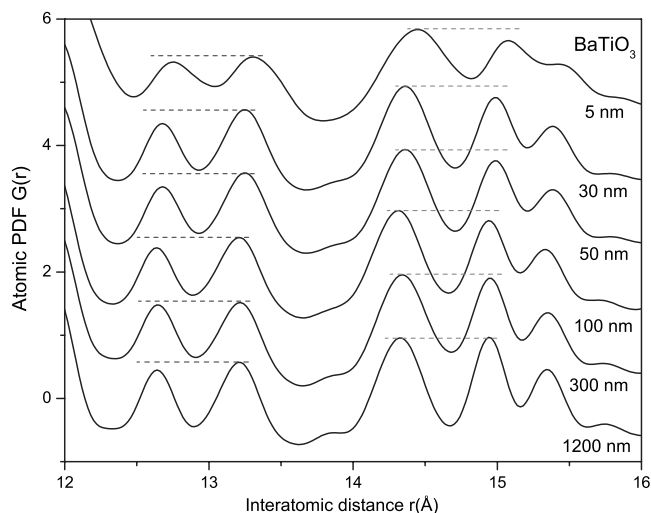


FIG. 7. Higher- r part of the experimental atomic PDFs for submicron- and nano-sized BaTiO₃ (shifted upward for clarity). The ratio of the intensities of the very well resolved PDF peaks centered at 12.7 and 13.3 Å, which are not related to Ti atoms, does not change substantially with the particle size. The ratio of the intensities of the similarly very well resolved PDF peaks centered at 14.3 and 14.9 Å, which are related to atomic correlations involving Ti atoms, changes substantially in a systematic way. The horizontal broken lines are a guide to the eye.

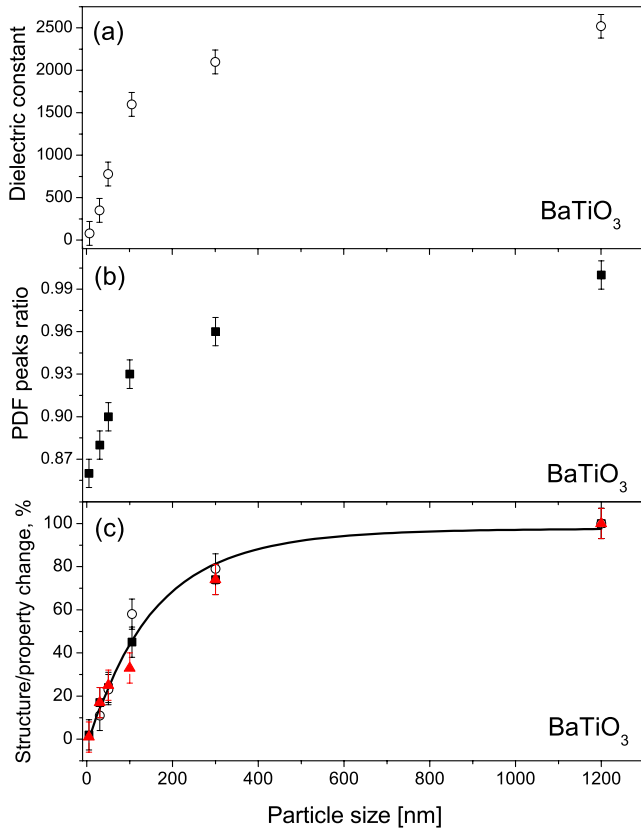


FIG. 8. (Color online) Dielectric constant of submicron- and nano-sized BaTiO_3 (a). Ratio of the intensities of the 14.3 and 14.9 Å peaks in the experimental PDFs for submicron- and nano-sized BaTiO_3 (b). The same data are plotted together with the loss in resolution of the 10 Å PDF doublet (triangles in red) in terms of relative (%) changes. The quantities are seen to decay exponentially (solid line) with the physical size of BaTiO_3 (c).

distorted/polar Ti-O_6 octahedra, i.e., of the long-range, tetragonal-type atomic arrangement, as reflected by the changing ratio of the intensities of 14.3 and 14.9 Å PDF peaks, and the loss of ferroelectricity, as reflected by the diminishing dielectric constant, are continuous processes that mirror each other exactly. When considered in terms of relative changes, both quantities are seen to collapse on a single structure/property vs system size curve that may be very well described by a first-order decaying exponent. To reveal the force driving the exponential decay of ferroelectricity in submicron- and nano-sized perovskites, we looked at another distinctive feature of their atomic ordering, i.e., the presence of substantial structural disorder, in more detail. This disorder is seen as an extra, i.e., beyond the usual thermal broadening of the PDF peaks. The extra broadening increases progressively with the reduction in the particle/grain size leading, for example, to a gradual merging of the two components of the PDF doublet centered at 10 Å (see Fig. 3). Note that doublet is one of the PDF features that do not change its shape substantially between the cubic and tetragonal phases of perovskites. As can be seen in Fig. 8(c), the splitting of the two components of the PDF doublet at 10 Å, i.e., the distinctiveness of the corresponding atomic coordination spheres, decays exponentially with the physical size

of BaTiO_3 . An exponential smearing of the PDF peak intensity distribution is a picture seen in order-disorder processes as, for example, fast melting of solids.²¹ In crystallography it is described by the so-called Debye-Waller factor,²² implying rms displacements that increase linearly with the diminishing system size. The rms fluctuations in nanosized perovskites are indeed rather substantial. For example in 5 nm BaTiO_3 , they amount to ~ 0.05 Å for interatomic distances of the order of 10 Å. Atomic positional disorder of such a magnitude is fully capable of destroying the long-range correlations between fine structural features such as the titanium off-center displacement [$\sim 0.03(5)$ Å for 5 nm BaTiO_3] in perovskites. This will inevitably lead to a deterioration of all cooperative properties, such as ferroelectricity, that need extended structural coherence/periodicity in order to evolve. Here it should be noted that our XRD/PDF data do not indicate the coexistence of different phases within the same perovskite grain/particle such as a tetragonal/ferroelectric core and a cubic-type/paraelectric layer/shell. Thus they are inconsistent with previous studies suggesting a transition between such phases taking place at some “critical” system size or a progressive shrinkage of the ferroelectric core with decreasing particle/grain size.²³ On the contrary, our results clearly show that Ti-O_6 octahedra are always distorted in submicron- and nano-sized BaTiO_3 and the material preserves its tetragonal-type lattice atomic ordering within at least 3 unit cells (~ 12 Å, see Fig. 5). A similar behavior has been observed in ultrathin perovskite films as well.⁸ Clearly, a functionally disrupted or disordered region close to the surface/interface of very small (e.g., nanosize) perovskite particles/layers may exist and affect adversely their ferroelectric properties. The presence and characteristics of such a region, however, are very much preparation technique and/or postprocessing dependent, as shown in several recent studies.^{3,4,6,10,11} That is why any realistic consideration of the behavior of ferroelectric perovskites of submicron size should always take into account the increased lattice positional disorder, and consider other size-related effects only if and up to the extent that they are really present.

IV. CONCLUSION

In summary, electronic industry relying on ferroelectric perovskites seems to face a hurdle just like semiconductor transistor industry does:²⁴ that is, the increased atomic positional disorder in systems confined to a small physical size. However, this is not a fundamental limit. The ferroelectricity does not disappear abruptly at a particular system size. It just weakens gradually and it is up to smart technological solutions to restore it by enforcing the translational periodicity of distorted Ti-O_6 octahedra well beyond a few unit cells of the perovskite lattice. Good results for thin perovskite films have already been obtained by using substrates that provide biaxial strain, enhancing the tetragonal ordering and, hence, the remanent polarization.²⁵ Nanosized capacitors may benefit from electrodes that both provide good screening of the

unbalanced surface charges²⁶ and enforce longer-range correlations between the atomic displacements responsible for the polarization in ferroelectrics.^{25,27} Effective technological solutions for submicron/nanosized loose powders and compacted ceramics are yet to be found. The success of future efforts along this line will require a precise characterization of the 3D structure of perovskites of very small physical size. As demonstrated here, high-energy XRD and atomic PDFs may accomplish this nontrivial task with success.

ACKNOWLEDGMENTS

This work was supported in part by CMU through Grant No. REF C602281. Use of the Advanced Photon Source was supported by the U.S. Department of Energy, Office of Science, Office of Basic Energy Sciences, under Contract No. DE-AC02-06CH11357. One of the authors (V.P.) is thankful to S. Pradhan and M. Gateshki for help in the XRD data analysis and useful discussions.

*Author to whom correspondence should be addressed; petkov@phy.cmich.edu

†v.buscaglia@ge.ienl.cnr.it

- ¹A. S. Bhalla, R. Gou, and R. Roy, *Mater. Res. Innovations* **4**, 3 (2000).
- ²N. Setter, D. Damjanovic, L. Eng, G. Fox, S. Gevorgian, S. Hong, A. Kingon, H. Kohlstedt, N. Y. Park, G. B. Stephenson, I. Stolitchnov, A. K. TagansteV, D. V. Taylor, T. Yamada, and S. Streiffer, *J. Appl. Phys.* **100**, 051606 (2006).
- ³T. M. Shaw, S. Trolier-McKinstry, and P. C. McIntyre, *Annu. Rev. Mater. Sci.* **30**, 263 (2000); M. H. Frey and D. A. Payne, *Appl. Phys. Lett.* **63**, 2753 (1993); T. Ohno, D. Suzuki, H. Suzuki, and T. Ida, *J. Soc. Powder Technol. Jpn.* **41**, 86 (2004).
- ⁴M. H. Frey, Z. Xu, P. Han, and D. A. Payne, *Ferroelectrics* **206**, 337 (1998).
- ⁵G. Arlt, D. Hennings, and G. de With, *J. Appl. Phys.* **58**, 1619 (1985); T. Takeuchi, C. Capiglia, N. Balakrishnan, Y. Takeda, and H. Kageyama, *J. Mater. Res.* **17**, 575 (2002); X. Deng, X. Wang, H. Wen, L. Chen, and L. Li, *Appl. Phys. Lett.* **88**, 252905 (2006).
- ⁶M. T. Buscaglia, M. Viviani, V. Buscaglia, L. Mitoseriu, A. Testino, P. Nanni, Z. Zhao, M. Nygren, C. Harnagea, D. Piazza, and C. Galassi, *Phys. Rev. B* **73**, 064114 (2006).
- ⁷T. Tybell, C. H. Ahn, and J.-M. Triscone, *Appl. Phys. Lett.* **75**, 856 (1999); C. H. Ahn, K. M. Rabe, and J.-M. Triscone, *Science* **303**, 488 (2004).
- ⁸D. D. Fong, G. B. Stephenson, S. K. Streiffer, J. A. Eastman, O. Auciello, P. H. Fuoss, and C. Thompson, *Science* **304**, 1650 (2004).
- ⁹W. L. Zhong, Y. G. Wang, P. L. Zhang, and B. D. Qu, *Phys. Rev. B* **50**, 698 (1994); S. Li, J. A. Eastman, Z. Li, C. M. Foster, R. E. Newnham, and L. E. Cross, *Phys. Lett. A* **212**, 341 (1996); S. Lin, T. Lü, Ch. Jin, and X. Wang, *Phys. Rev. B* **74**, 134115 (2006).
- ¹⁰L. J. Sinnamon, M. M. Saad, R. W. Bowman, and J. M. Gregg, *Appl. Phys. Lett.* **81**, 703 (2002); A. Yu. Emelyanov, N. A. Pertsev, S. Hoffmann-Eifert, U. Böttger, and R. Waser, *J. Electroceram.* **9**, 5 (2002); A. G. Zembilgotov, N. A. Pertsev, and R. Waser, *J. Appl. Phys.* **97**, 114315 (2005).
- ¹¹Z. Zhao, V. Buscaglia, M. Viviani, M. T. Buscaglia, L. Mitoseriu, A. Testino, M. Nygren, M. Johnsson, and P. Nanni, *Phys. Rev. B* **70**, 024107 (2004).
- ¹²G. Gerra, A. K. Tagantsev, N. Setter, and K. Parlinski, *Phys. Rev. Lett.* **96**, 107603 (2006); M. Stengel and N. Spaldin, *Nature (London)* **443**, 679 (2006).
- ¹³A. A. Sirenko, C. Bernhard, A. Golnik, A. M. Clark, J. Hao, W. Si, and X. X. Xi, *Nature (London)* **404**, 373 (2000).
- ¹⁴T. Ostapchuk, J. Petzelt, M. Savinov, V. Buscaglia, and L. Mitoseriu, *Phase Transitions* **79**, 361 (2006).
- ¹⁵V. Petkov, P. Y. Zavalij, S. Lutta, M. S. Whittingham, V. Parvanov, and S. D. Shastri, *Phys. Rev. B* **69**, 085410 (2004); V. Petkov, T. Ohta, Y. Hou, and Y. Ren, *J. Phys. Chem. C* **111**, 714 (2007).
- ¹⁶G. H. Kwei, A. C. Lawson, S. J. L. Billinge, and S.-W. Cheong, *J. Phys. Chem.* **97**, 2368 (1993).
- ¹⁷V. Petkov, M. Gateshki, M. Niederberger, and Y. Ren, *Chem. Mater.* **18**, 814 (2006).
- ¹⁸T. Egami and S. J. L. Billinge, *Underneath the Bragg Peaks* (Pergamon, Amsterdam, 2003).
- ¹⁹A. I. Frenkel, Y. Feldman, V. Lyahovitskaya, E. Wachtel, and I. Lubomirsky, *Phys. Rev. B* **71**, 024116 (2005); Y.-I. Kim, J. K. Jung, and K. S. Ryu, *Mater. Res. Bull.* **39**, 1045 (2004).
- ²⁰M. H. Frey and D. A. Payne, *Phys. Rev. B* **54**, 3158 (1996); V. Buscaglia, M. T. Buscaglia, M. Viviani, T. Ostapchuk, I. Gregora, J. Petzelt, L. Mitoseriu, P. Nanni, A. Testino, R. Calderone, C. Harnagea, Z. Zhao, and M. Nygren, *J. Eur. Ceram. Soc.* **25**, 3059 (2005); X. Wang, X. Deng, H. Wen, and L. Li, *Appl. Phys. Lett.* **89**, 162902 (2006); Y. Shiratori, C. Pithan, J. Dornseiffer, and R. Waser, *J. Raman Spectrosc.* **38**, 1300 (2007).
- ²¹B. J. Siwick, J. R. Dwyer, R. E. Jordan, and R. J. D. Miller, *Science* **302**, 1382 (2003); K. J. Gaffney, A. M. Lindenberg, J. Larsson, K. Sokolowski-Tinten, C. Blome, O. Synnergren, J. Sheppard, C. Coleman, A. G. MacPhee, D. Weinstein, D. P. Lowney, T. Allison, T. Matthews, R. W. Falcone, A. L. Cavalieri, D. M. Fritz, S. H. Lee, P. H. Bucksbaum, D. A. Reis, J. Rudati, A. T. Macrander, P. H. Fuoss, C. C. Kao, D. P. Siddons, R. Pahl, K. Moffat, J. Als-Nielsen, S. Duesterer, R. Ischebeck, H. Schlarb, H. Schulte-Schrepping, J. Schneider, D. von der Linde, O. Hignette, F. Sette, H. N. Chapman, R. W. Lee, T. N. Hansen, J. S. Wark, M. Bergh, G. Huld, D. van der Spoel, N. Timneanu, J. Hajdu, R. A. Akre, E. Bong, P. Krejčík, J. Arthur, S. Brennan, K. Luening, and J. B. Hastings, *Phys. Rev. Lett.* **95**, 125701 (2005).
- ²²M. F. Thorpe, *Local Structure from Diffraction* (Plenum, New York, 1998).
- ²³K. Uchino, E. Sadanaga, and T. Hirose, *J. Am. Ceram. Soc.* **72**, 1555 (1989); M. Tanaka and Y. Makino, *Ferroelectr., Lett. Sect.* **24**, 13 (1998); R. Böttcher, C. Klimm, D. Michel, H.-C. Sempelhack, G. Völkel, H.-J. Gläsel, and E. Hartmann, *Phys. Rev. B* **62**, 2085 (2000).
- ²⁴R. W. Keyes, *Rep. Prog. Phys.* **68**, 2701 (2005).
- ²⁵K. J. Choi, M. Biegalski, Y. L. Li, A. Sharan, J. Schubert, R.

Uecker, P. Reiche, Y. B. Chen, X. Q. Pan, V. Gopalan, L.-Q. Chen, D. G. Schlom, and C. B. Eom, *Science* **306**, 1005 (2004).

²⁶The unbalanced surface charge is expected to cause a considerable depolarization field in perovskites only a few nanometers in size. However, that field is likely to be of somewhat a random character given the large degree of structural disorder they ex-

hibit. The situation may vary from sample to sample especially when a “support” for the perovskite material is used.

²⁷J. Paul, T. Nishimatsu, Y. Kawazoe, and U. V. Waghmare, *Phys. Rev. Lett.* **99**, 077601 (2007); R. Plonka, R. Dittmann, N. A. Pertsev, E. Vasco, and R. Waser, *Appl. Phys. Lett.* **86**, 202908 (2005).